A high-resolution marine mercury model MITgcm-ECCO2-Hg with online biogeochemistry

Siyu Zhu[1], Peipei Wu[1], Siyi Zhang[2], Oliver Jahn[3], Yanxu Zhang[1,4]

[1]Joint International Research Laboratory of Atmospheric and Earth System Sciences, School of Atmospheric Sciences, Nanjing
University, Nanjing 210023, China
[2]Department of Environmental Systems Science, ETH Zurich, Zurich, Switzerland
[3]Department of Earth, Atmospheric and Planetary Sciences, Massachusetts Institute of Technology, Cambridge, MA 02139,
USA
[4]Frontiers Science Center for Critical Earth Material Cycling, Nanjing University, Nanjing 210023, China

Correspondence to: Yanxu Zhang (zhangyx@nju.edu.cn)

Abstract. Mercury (Hg) is a global persistent contaminant. Modeling studies are useful means of synthesizing a current understanding of the Hg cycle. Previous studies mainly use coarse-resolution models, which makes it impossible to analyze the role of turbulence in the Hg cycle and inaccurately describes the transport of kinetic energy. Furthermore, all of them are coupled with offline biogeochemistry, so they cannot respond to short-term variability in oceanic Hg concentration. Here we use a high-resolution (horizontal resolution is 1/5°) ocean model (MITgcm-ECCO2, high-resolution-MITgcm) coupled with the online biogeochemistry of Darwin project to simulate the global Hg cycle. The finer portrayal of surface Hg concentrations in estuarine and coastal areas, strong western boundary flow and upwelling areas, and concentration diffusion as vortex shapes demonstrate the effects of turbulence that are neglected in previous models. Ecological events such as algal blooms can cause a sudden enhancement of phytoplankton biomass and chlorophyll concentrations, which can also result in a dramatic change in particle-bound mercury (Hg_{aq}^P) sinking flux at the same time in our simulation. In the global estuary region, the inclusion of riverine Hg input in the high-resolution model allows us to reveal the outward spread of Hg in an eddy shape driven by fine-scale ocean currents. With faster current velocities and diffusion rates, our model captures the transport and mixing of Hg from river discharge in a more accurate and detailed way and improves our understanding of Hg cycle in the ocean.

1 Introduction

Mercury (Hg) is a potent neurotoxin that poses health risks to the global population and causes substantial economic losses regulated by Minamata Convention (Zhang et al., 2021). Anthropogenic emissions of Hg from mining and coal combustion severely disturb the biogeochemical cycling of Hg (Nriagu, 1993; Lacerda, 1997; Pacyna et al., 2010; Streets et al., 2011). Mercury can be transported and recycled in the global ocean, atmosphere, and land until buried in deep-sea sediment (Outridge et al., 2018). The ocean is an important part of the biogeochemical cycle of Hg, evidenced by the large air-sea exchange flux and complex biogeochemical transformation that have direct implications for human exposure to Hg through seafood consumption.

The source of marine Hg contains atmospheric deposition, riverine discharge, benthic sediments, and hydrothermal vents (Mason et al., 2012). The air−sea exchange of Hg is driven by the concentration gradients between the atmospheric and seawater interface (Soerensen et al., 2013), which are influenced by atmospheric deposition of Hg_{aq}^{II} and photochemical and

35   dark reduction/oxidation of Hg_{aq}^{II}/Hg_{aq}^{0} in the seawater (Costa and Liss, 1999; Gardfeldt et al., 2001; Andersson et al., 2011; Ci et al., 2016). In the mixed layer, the reduction reactions of Hg_{aq}^{II} to Hg_{aq}^{0} and high vapor pressure of Hg_{aq}^{0} makes it emitted into the atmosphere again (Mason et al., 1995; Amyot et al., 1997; Rolfhus and Fitzgerald, 2001). Hg_{aq}^{II} can be absorbed by suspended organic-rich particulate matter to produce Hg_{aq}^{P} (Fitzgerald et al., 2007). Then Hg_{aq}^{P} sinks to the subsurface ocean as part of the biological pump and is released in the dissolved phase by the remineralization of sinking particles (Strode et al.,

40   2010).

Marine Hg models have been developed to improve our understanding of the cycling of oceanic Hg. One of the earliest marine model developments was a 2-D slab ocean model coupled with the atmosphere (GEOS-Chem), which considered the red-ox chemistry and transport of inorganic Hg (Strode et al., 2007; Selin et al., 2008; Soerensen et al., 2010). Three-dimensional marine Hg models were applied to simulate the spatiotemporal dynamics of inorganic Hg species in the ocean (Zhang et al.,

45   2014a; Zhang et al., 2014b; Bieser and Schrum, 2016). Later models were developed with improved ocean biogeochemistry. For example, Zhang et al. (2020) and Rosati et al. (2022) coupled Hg cycling with a biogeochemical and ecological model, considering the uptake to and release of Hg from marine biota. The lasted developed biogeochemical multi-compartment model for Hg cycling MERCY v2.0 developed by (Bieser et al., 2022), includes all currently known processes controlling marine Hg cycling.

50   One limitation of earlier models is their inaccurate representation of eddies due to the relative coarse model resolutions. For example, previous studies that simulated the chemistry and transport using the MIT General Circulation Model (MITgcm) had a horizontal resolution of 1° over the global ocean, with improved resolution only in the Arctic and equator (Zhang et al., 2015; Zhang et al., 2020; Huang and Zhang, 2021). The Nucleus for European Modeling of the Ocean (NEMO) framework version 3.1 was developed by Semeniuk and Dastoor (2017), and it adopted a tripolar, variable resolution grid (called ORCA2), which

55   resolves less than a degree in the tropics, the Mediterranean Sea, and the Red Sea and 2° elsewhere. The dissipation of kinetic energy in the turbulent boundary layers and the ocean interior at much smaller scales than the model grid (Wunsch and Ferrari, 2004), and the turbulent mixing controls their transport and storage (Sarmiento et al., 2004), which cannot be accurately represented by coarse-resolution ocean models. In addition, Hg cycling in coastal waters is highly sensitive to anthropogenic disturbances and climate-induced changes (Jonsson et al., 2017; Obrist et al., 2018). The coarse model resolution also cannot

60   reflect the transport and mixing conditions at estuaries and continental shelves. Therefore, models with higher resolutions or parameterizations of eddies are required to improve the accuracy of the simulation of the Hg cycle in the ocean.

Besides, the chemistry of Hg and biogeochemistry is offline so it couldn't reflect the short-term changes of biogeochemistry, such as algal/phytoplankton bloom events that can significantly impact phytoplankton and zooplankton structure and aquatic environments (Amorim and Moura, 2021). Phytoplankton is the base of pelagic food webs and has been found to

65 bioaccumulate 105 times more Hg than successive trophic transfers (Watras et al., 1998; Moye et al., 2002; Pickhardt and
Fisher, 2007). Therefore, small changes in phytoplankton may significantly impact overall Hg bioaccumulation in the entire
system. In the study of Luengen and Russell Flegal (2009), total Hg concentrations decreased when the bloom decayed,
possibly because particles (i.e., phytoplankton) with low Hg concentrations were lost from the water column. Another research
showed that degradation and sedimentation of algal debris will increase the organic matter load in the sediment (Macalady et

70 al., 2000), which could impact particle-bound Hg levels.

We develop a new simulation for Hg chemistry, transport, and trophic transfer within the high-resolution MITgcm combined
with an ecology and biogeochemistry model (the Darwin project; http://darwinproject.mit.edu). The model has a horizontal
resolution of 1/5°, allowing the formation of eddies and narrow currents (Menemenlis et al., 2008). The eddy-permitting and
delicate resolutions model allows us to examine the influence of physical dispersal, which is a major way of marine substance

75 transport on the transmission of marine Hg, especially over western boundary currents and coastal upwelling regions. We also
investigate the influence of online biogeochemistry on Hg chemistry. Finally, we study the fate of the riverine discharge of Hg
and the impact of nutrients over coastal waters near big river mouths on the transport of coastal Hg.

2 Model description

2.1 High-Resolution MITgcm

80 We use MITgcm to simulate the transport and chemistry of Hg in the global ocean. The physical component of the model uses
the ECCO2 physical configuration, which addresses mesoscale features in the tropics and allows eddies in subpolar regions
where the deformation radius is comparable to the grid scale. It employs the cube-sphere grid projection, permitting relatively
even grid spacing throughout the domain, and avoids polar singularities (Adcroft et al., 2004). Each face of the cube consists
of 510 grid cells with an average horizontal grid spacing of 18 km. There are 50 vertical levels ranging from 10 m near the

85 surface to approximately 450 m at a maximum model depth of 6150 m in the model. The ECCO2 project provides the best-
possible, global, time-evolving synthesis of the most available ocean and sea-ice data at a resolution permitting ocean eddies
(Menemenlis et al., 2008).

Our model includes three Hg tracers: dissolved elemental (Hg_{aq}^0), dissolved divalent (Hg_{aq}^{II}), and particle-bound mercury
(Hg_{aq}^P). We take atmospheric deposition flux and atmospheric GEM (gas element mercury) concentrations as the upper

90 boundary conditions for Hg^{II} and Hg^0, respectively from Zhang and Zhang (2022) and Horowitz et al. (2017). The model
takes the initial conditions of ocean Hg concentration from Zhang et al. (2020), which is linearly interpolated to the high-
resolution MITgcm model grid. A 6-month free-running simulation is conducted.

2.2 Ocean Biogeochemistry and Ecology

We use a coupled ocean plankton ecology and biogeochemistry model (the Darwin project) within the high-resolution MITgcm,
95 simulating the production and growth of different plankton species and organic carbon remineralization in the marine water
column. The Darwin project includes ocean biogeochemistry and ecological variables (e.g., POC and DOC), Hg_{aq}^P is
scavenged by POC to the deep sea through the biological pump. The biogeochemical and biological tracers interact through
organic matter formation, transformation, and remineralization. This model simulates the cycling of nutrients (C, N, P, Si, and
Fe), phytoplankton growth, zooplankton grazing, and mortality (Dutkiewicz et al., 2009; Ward et al., 2014; Zhang et al., 2015).
100 There are 51 plankton types (35 phytoplankton and 16 zooplankton) in the complex plankton community, phytoplankton is
divided into six functional groups: prokaryotes, picoeukaryotes, coccolithophores (that calcify), diazotrophs (cyanobacteria),
diatoms (that utilize silicic acid), and mixotrophic dinoflagellates. The six representative categories of phytoplankton have
different sizes, growth rates, grazing, sinking, and affinity to nutrients and other physiological parameters (Kuhn et al., 2019).
The online coupled variables coupled with the Darwin project are used to parameterize the Hg chemistry, including deposition
105 and escape of Hg in the surface ocean and photochemical and biochemical redox of Hg in seawater. This is explained in more
detail in the following sections.

2.3 Air-sea exchange

The ocean model is coupled to the atmosphere by receiving the atmospheric deposition of Hg^{II} and Hg^0. Atmospheric
deposition of Hg^{II} is the main input of Hg to the surface environment (Amos et al., 2012), which is largely affected by the
110 amount and type of precipitation and is also influenced by the wind, through controlling the removal of Hg by sea-salt particles.
The air-sea exchange of Hg^0 is mainly evasion from the ocean to the atmosphere (Mason et al., 2017), which is driven by the
concentration gradient at the interface between the atmosphere and seawater (Soerensen et al., 2013) and the piston velocity is
a function of wind speed and temperature parameterized by Nightingale et al. (2000). The air-sea exchange of Hg^0 is calculated
following Strode et al. (2007):

$$115 \quad F_{evasion} = k_w \times \left(\left[Hg_{aq}^0 \right] - H \left[Hg_{air}^0 \right] \right), \tag{1}$$

where k_w is the gas exchange velocity (piston velocity), and H is the dimensionless temperature-dependent Henry's Law
constant. k_w is related to the sea ice fraction and the instantaneous wind speed. Through the above, the spatial distribution of
the evasion flux is controlled by the supersaturation of Hg^0 concentrations, and wind speeds, and is associated with sea ice
fraction in some regions. The calculation process variables are online coupled, we could simulate a time-sensitive source and
120 sink of marine Hg.

2.4 Hg Chemistry

In the euphotic layer of the ocean, the photo-chemistry and biological-mediated oxidation and reduction reactions between Hg_{aq}^{0} and Hg_{aq}^{II} in our model are based on (Zhang et al., 2014a), with some associated variables are replaced by the ones coupled online. The photochemical oxidation and photochemical reduction first-order rate constants (k1 and k2 in Table 1) are

125   proportional to short-wave radiation at the sea surface (RAD in Table 1), which is coupled by online variables from the Darwin project:

$$RAD = \int_{0}^{nlam} PAR(1-ice) \times 0.2174 / 0.4 , \tag{2}$$

where PAR is each band of short-wave radiation at the sea surface, and $nlam$ is the total band of PAR. The unit of PAR is $ein\ \mathrm{m}^{-2}\ \mathrm{d}^{-1}$, so it needs to transfer to $W\ \mathrm{m}^{-2}$ by multiplying a coefficient of 0.2174. And the PAR to total upward shortwave

130   radiation is 40%, so we also need to divide this scale coefficient.

The biological oxidation and reduction processes first-order rate constants (k3 and k4 in Table 1) are proportional to the microbial remineralization of particulate organic carbon (OCRR in Table 1). Biologically mediated Hg redox reactions are attributed to the activities of heterotrophic and chemotrophic microorganisms (Mason et al., 1995; Monperrus et al., 2007). Zhang et al. (2014b) scale the biologically mediated reduction of Hg_{aq}^{II} to Hg_{aq}^{0} (k4) to OCRR, which is a measure of the

135   microorganism activity. Here the online variable OCRR is one of the focuses of the high-resolution MITgcm coupled with and Darwin project.

$$OCRR = (re\min DOC + re\min POC) , \tag{3}$$

where reminDOC and the reminPOC are the remineralization part of DOC and POC, respectively.

Partitioning of Hg_{aq}^{II} onto particulate organic carbon (POC) to form HgP, then HgP sinking to deeper waters as part of the

140   biological pump in the ecology and biogeochemistry model. Assuming that Hg_{aq}^{II} and Hg_{aq}^{P} can exchange to each other reversibly and the ratio of them (k_d) is proportional to the local particulate organic carbon (POC) level (Zhang et al., 2014b). The POC pool includes both detritus and living phytoplankton, as partitioning of inorganic Hg_{aq}^{II} to living and dead cells are similar (Pickhardt and Fisher, 2007).

$$F_{Hg}{}^{P} = (Hg_{aq}^{P} \times F_{poc+phy}) / (sumPOC + sumPhyto + sumZoop) , \tag{4}$$

145   the sinking flux of HgP(aq) ($F_{Hg^{p}}$, $mol\ \mathrm{m}^{-2}\ \mathrm{s}^{-1}$) is assumed to be proportional to the sinking flux of POC and phytoplankton ($F_{poc+phy}$, $mol\ \mathrm{m}^{-2}\ \mathrm{s}^{-1}$). The sumPOC, the sumPhyto, and the sumZoop are the sum of surface chlorophyll concentrations (unit, $mg\ \mathrm{chl\ a\ m}^{-3}$), biomass concentration of phytoplankton (unit, $mmol\ \mathrm{C\ m}^{-3}$), and biomass concentration of zooplankton (unit, $mmol\ \mathrm{C\ m}^{-3}$) respectively. These parameters are coupled with the Darwin project.

2.5 Riverine Hg

150   Most riverine Hg transported to the ocean is associated with particles (Sonke et al., 2018), and Zhang et al. (2015) infer most of the river Hg discharged to the ocean is refractory. We use the riverine discharge Hg inventory from Liu et al. (2021), including riverine dissolved and particulate Hg. A separate refractory HgP tracer is used to simulate the particulate Hg from rivers (HgPR), reflecting its strong combination with terrestrial source POC. The refractory HgP is released into the dissolved phase only when the organic carbon is remineralized. Furthermore, we use the nutrient export by river from WaterSheds 2

155   (NEWS 2) developed by Mayorga et al. (2010), which is a global, spatially explicit, multi-element, and multi-form model of nutrient exports by rivers. Global annual export of total N (TN), P (TP), and organic C (TOC) from rivers is estimated to be 44.9 Tg N, 9.04 Tg P, and 317 Tg C, respectively. The distribution among forms for global exoreic exports varies by the element, with DIN (43.7%) and PN (31.2%) dominating nitrogen exports, PP (76.5%) and DIP (16.7%) dominating phosphorus exports, and DOC (53.9%) dominating organic carbon exports. By incorporating these riverine nutrients, we can assess their

160   impact on the ocean ecosystem, including chlorophyll and marine plankton, and their influence on the cycling and sinking of particle-bound Hg.

Table 1. Description of the Main Processes and Input Fields Used in the MITgcm-Hg Simulation

Parameter	Description	Reference or Source
F_{dep}	Atmospheric wet deposition flux of Hg^{II} to the ocean, $mol\ m^{-2}\ s^{-1}$	Zhang and Zhang (2022)
$F_{evasion}$	Net evasion flux of Hg^0 across the air-sea interface, $mol\ m^{-2}\ s^{-1}$	Model results
$F_{riverine}$	Riverine input of Hg, mol $m^{-2}\ s^{-1}$	Liu et al. (2021)
k_1	Photooxidation of Hg^0_{aq} to Hg^{II}_{aq} $k_1 = k_{photo-ox} \times RAD$ $k_{photo-ox} = 4.7 \times 10^{-6}$	Soerensen et al. (2010), updated by Zhang et al. (2015)
k_2	Photoreduction of Hg^{II}_{aq} to Hg^0_{aq} $k_2 = k_{photo-re} \times RAD$ $k_{photo-re} = 1.56 \times 10^{-6}$	Soerensen et al. (2010), updated by Zhang et al. (2015)
k_3	Biological oxidation of Hg^0_{aq} to Hg^{II}_{aq} $k_3 = k_{bio-ox} \times OCRR$ $k_{bio-ox} = 9.9 \times 10^{-7}$	Soerensen et al. (2010), updated by Zhang et al. (2015)

k_4	Biological reduction of Hg_{aq}^{II} to Hg_{aq}^0 $$k_4 = k_{bio-re} \times OCRR$$ $$k_{bio-re} = 6.2 \times 10^{-7}$$	Soerensen et al. (2010), updated by Zhang et al. (2015)
k_{dark}	Dark oxidation of Hg_{aq}^0 to Hg_{aq}^{II}	Soerensen et al. (2010), updated by Zhang et al. (2015)
POC	Particulate organic carbon concentration in seawater, $mmol$ C m^{-3}	Darwin model variable
DOC	Dissolved organic carbon concentration in seawater, $mmol$ C m^{-3}	Darwin model variable
Chl	Surface chlorophyll concentrations, mg chl a m^{-3}	Darwin model variable
Phyto	Biomass (in carbon content) concentration of phytoplankton, $mmol$ C m^3	Darwin model variable
Zoop	Biomass (in carbon content) concentration of zooplankton, $mmol$ C m^{-3}	Darwin model variable
OCRR	Organic carbon remineralization rate	Darwin model variable
RAD	Short-wave radiation flux, W m^{-2}	Darwin model variable
PAR	each band of short-wave radiation at the sea surface	Darwin model variable
Ice	Fraction of surface sea ice (0-1)	Darwin model variable

3 Model evaluation

3.1 Global inorganic Hg distribution in surface ocean

The global average daily inorganic Hg (Hg^0 and Hg^2) distribution in surface ocean derived from our high-resolution-MITgcm/Hg simulation compares with the observed total Hg concentrations in global surface seawater (Figure 1). Our model takes into account the effects of temperature, ocean current motion, turbulent mixing, and nearshore topography, all of which contribute to differences in oceanic Hg distribution. As a result, we obtain a more refined global distribution of Hg at the ocean surface. Delicate simulations of inorganic Hg in the surface ocean reflect regional differences and eddy scale changes of concentration, which are aroused by ocean currents or geographical factors. Our high-resolution model shows more detailed changes and a clearer gradient between continent and ocean due to the narrower, swifter currents and strong shear, which can increase the efficiency of mixing. Overall, the distribution of inorganic Hg in our model is similar to that simulated in the

175   lower-resolution ECCO v4 MITgcm (Fig. S1). The modeled concentration of Hg (mean and standard deviation: 0.60 ± 1.41
      pM) is slightly lower than the observed concentration (0.87 ± 0.46 pM) in seawater. As we use a similar Hg chemistry and
      exchange scheme as previous models (Table 1), the difference in model results reflects a potential dependence of these
      parameters on model resolution. Besides, the various parameters of the ecosystem vary greatly between this study and previous
      ones (e.g., different community structures, etc.).
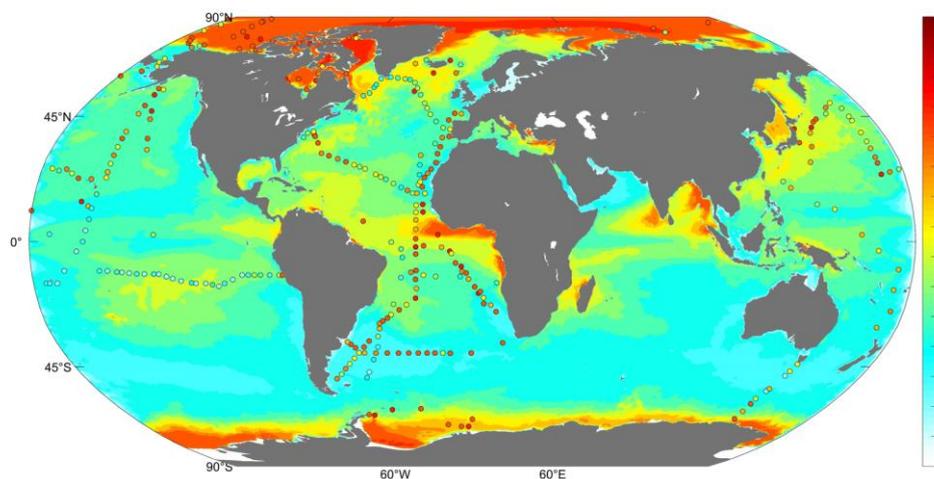
180

Figure 1. Global simulation of the daily mean total inorganic Hg (0-10 m depth; color, unit pM(10^{-9}mol m^{-3})) and observation of total inorganic Hg in the ocean surface (0-10 m depth; scatter, unit pM). Observations are from the North Pacific Ocean (Laurier et al., 2004), the Atlantic (Kuss et al., 2011), the Equator & South Atlantic (Mason and Sullivan, 1999), the North Atlantic (Mason et al., 1998; Mason et al., 2001; Bowman et al., 2015), the Southern Ocean (Cossa et al., 2011), and the Arctic Ocean (Kirk et al., 2008;
185   **Chaulk et al., 2011; Lehnherr et al., 2011; Heimbuerger et al., 2015).**

      The simulated total inorganic Hg shows greater global and regional differences compared to previous models. Variables
      coupled with online biogeochemistry are involved in the chemical production and consumption of inorganic Hg, resulting in
      modeled Hg concentrations that better match observations (the Hg^{II} deposition flux and Hg^0 evasion flux are shown in Fig.
      S2). Typically, observations are not continuous, and the values of certain adjacent observations may vary significantly. This
190   variability has been observed in the high-precision cruise data (Figure 2 Scattered points in red box). This indicates that the
      distribution of Hg in the real ocean is highly variable, but this variation was not apparent due to the resolution limits in the
      previous marine models. Figure 2 illustrates that high-resolution simulated results are closer to observations than previous
      lower-resolution models (Zhang et al., 2020). In the red box circled position, Figure 2. a(c) can replicate the significant
      difference in the observed data at nearby locations at the same time (or in a short time).
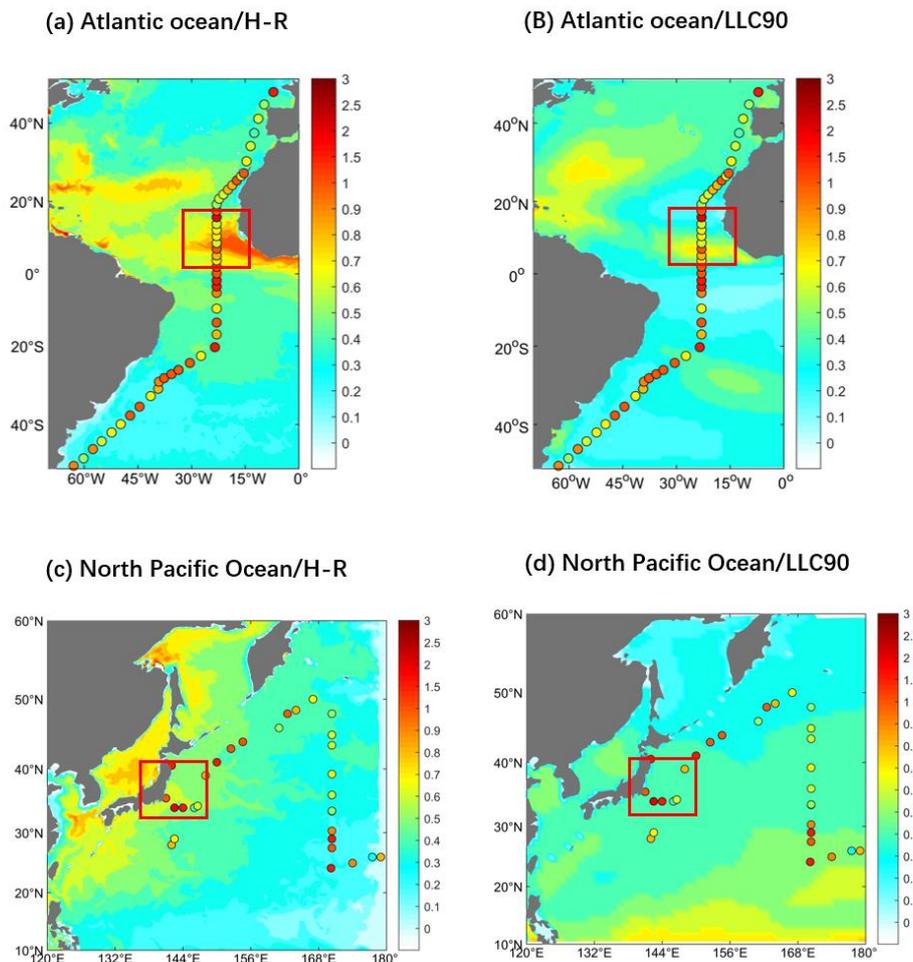
Figure 2. MITgcm simulation for total inorganic Hg results of high resolution (1/5°×1/5° horizontal) ECCO2 (H-R) and coarser (1°×1° horizontal) resolution ECCO v4 (LLC90) (0-10 m depth; color, unit pM, (Huang and Zhang, 2021)). The scatter is observations from two single high spatial precision cruises, (a,b) from Kuss et al. (2011) Atlantic Ocean observations in a month, and (c,d) from Laurier et al. (2004) North Pacific observations in a day(0-10 m depth; scatter, unit pM).

Ocean currents and turbulence play an important role in the physical transport of Hg. Strong upwelling occurs where the western boundary stream is strong or where cold and warm currents meet, which facilitates the horizontal and vertical exchange of Hg in the ocean, resulting in a heterogeneous distribution and drastic changes. In addition, the effect of turbulence across the ocean causes the spread of Hg in a vortical shape. The finer portrayal of inorganic Hg in Figure 3 demonstrates the influence of ocean currents and turbulence. The Kuroshio in the western Pacific Ocean and the Gulf Stream in the North Atlantic Ocean are the most powerful Western Boundary Currents in the world, and the western boundary flow region is the area with very active vortices and a fast flow rate. This region shows more significant concentration changes and clear eddy structures in the distribution of inorganic Hg compared to the surrounding ocean (Figure3.a and Figure3.b). Other areas in the distribution of Hg with significant changes are the Pacific and Atlantic equatorial regions, which are possibly influenced by the westward

Equatorial Warm Currents. Moreover, the transport and mixing of Hg are stronger and faster where cold and warm currents

210 meet (Figure3.b and Figure3.d). It was also found that cold currents have a milder effect on Hg transport and dispersion as

compared to warm currents (Figure3.c and Figure3.d).
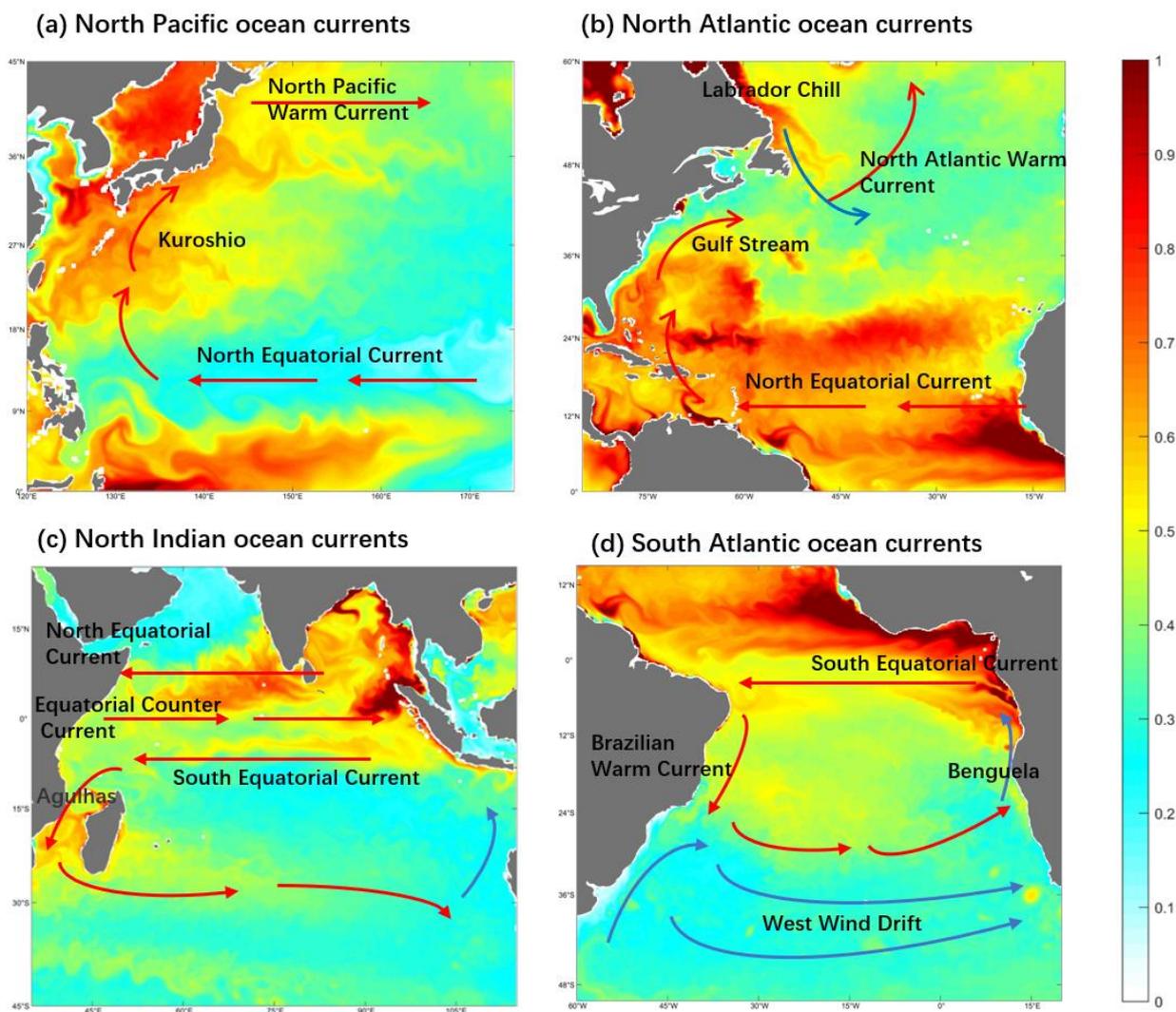
Figure 3. Total inorganic Hg Simulation of regions with ocean currents (0-10 m depth; color, unit pM). Zoom for (a) the Northwest Pacific Ocean, (b) the Northwest Atlantic Ocean, (c) the North Indian Ocean, and (d) the South Atlantic Ocean.

215 **3.2 Riverine Hg discharge**

Rivers are important sources of coastal Hg. We model Hg from rivers as a refractory tracer following Zhang et al. (2015).

Driven by the riverine input (1000 Mg a^{-1}, 893–1,224) from Liu et al. (2021), after transferring and mixing for six months in

our simulation (Figure 4), most of the Hg (93.7%) is buried in estuarine sediments (ocean depth < 55 m), while 6% is buried

in shelves (ocean depth between 55 m and 180 m), and less than 0.01% export to the open ocean (ocean depth >180 m). We model a higher percentage of refractory particulate oxidized Hg (HgPR) buried in estuarine sediments and less is buried in shelves and exports to the open ocean, compared with previous studies. For example, 72-73% buried in estuarine sediments, and 5-6.4% transported to the open ocean by Zhang et al. (2015) and Liu et al. (2021). Indeed, with a higher resolution, coastal currents can be resolved with river discharge being transferred along the seashores. In contrast, the coarse resolution model assumes even mixing at the first grid point for a long distance, leading to an overestimate of the transmission to distant oceans.
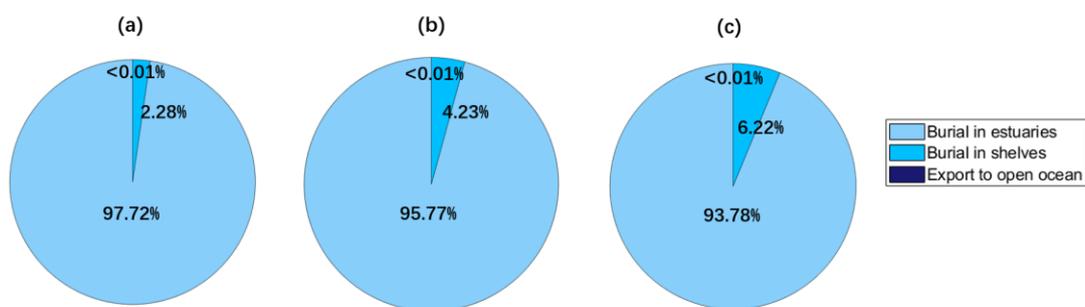
225

Figure 4. Global simulations of the fate of refractory particulate oxidized Hg (HgPR) discharged by rivers. Estuaries, shelves, and open oceans are defined as ocean regions with depth < 55 m, 55–185 m, and >185 m, respectively. Coastal ocean refers to estuaries and the shelf. (a)-(c) is the simulation results of the last day of 4-6 months, respectively.

The spatial distribution of riverine input refractory particulate oxidized Hg across the global ocean is driven by both variabilities in HgPR concentrations and suspended sediment discharges (Figure 5). Major rivers and highly contaminated systems are visible on the global chart (e.g., Yangtze, Amazon, Ganges). The high Hg discharges from Mexican rivers into the Pacific Ocean reflect the high total suspended sediment flux values, as previously described by (Liu et al., 2021). To gain a clearer understanding of the fate of HgPR discharge, we zoom in on the major river mouth regions for further investigation. The rivers selected for the analysis include the Rio Grande River in North America, the Yellow River, the Yangtze River, the Amur River, the Pearl River, and the Zigzag River in Asia, the Orinoco River and the Amazon River in South America, and the Congo River in Africa. We find that riverine inputs of HgPR to the coastal ocean have a limited impact on Hg concentrations in surface seawater beyond the shelf region. HgPR is transported to the left or right along the coast by the Coriolis force, the influence of currents and eddies leads to dispersion slightly further away from the coast.
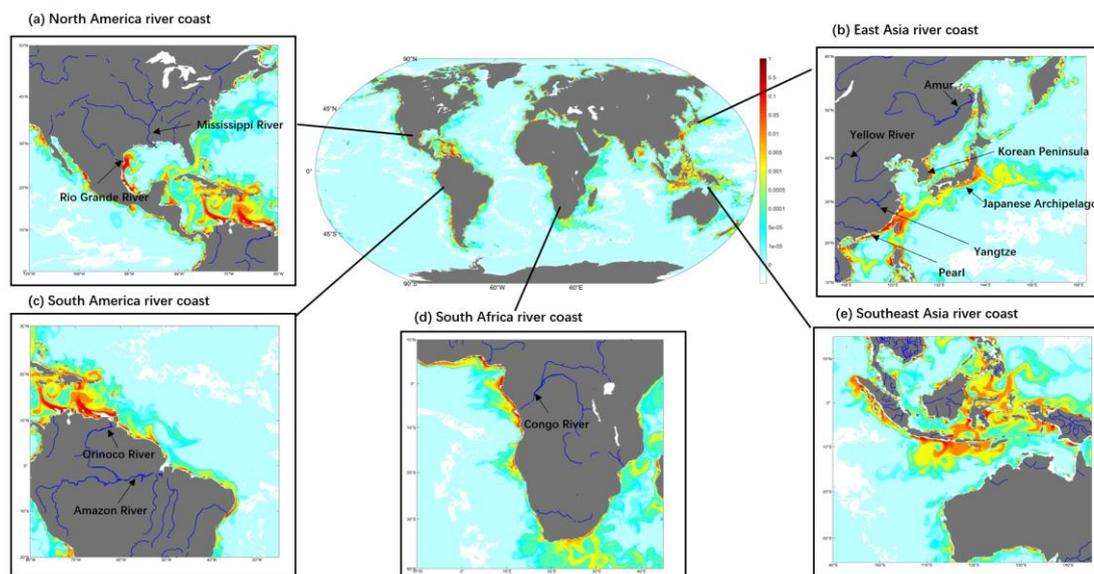
Figure 5. Global and coastal distribution of daily refractory particulate oxidized Hg (HgPR) on the last simulation day (0-10 m depth; color, unit pM). Zoom for (a) North American river coast, (b) East Asia river coast, (c) South American river coast (d) South African river coast, (e) Southeast Asia river coast.

In the case of the Amazon River, which is the largest exporter of freshwater and particulate matter to marine waters globally (Amos et al., 2014), generating up to a $1.3 \times 10^6\, km^2$ plume, and extensive muddy bottoms in the equatorial margin of South America (Moura et al., 2016). Our model results show that Hg discharges from the river are transported northwestward along the Brazilian continental shelf without significant offshore transport before intersecting the Equatorial Counter Current (Figure 5c). This is consistent with the model simulation by Zhang et al. (2015), but the plume we simulate is much finer and narrower due to the higher resolution of the model. This is also consistent with the observation (Mason and Sullivan, 1999), which shows that there is an apparent absence of a riverine Hg plume and low total Hg concentrations in the open Equatorial Atlantic Ocean near the Amazon River mouth

Hg exports from rivers are important to specific coastal areas, Liu et al. (2021) have raised further concerns about riverine Hg and a deeper understanding of the role of rivers in the global Hg cycle. The discharge of HgPR from rivers greatly impacts environmental pollution in coastal and shelf regions. Our model results show that HgPR is transported from the coast to the ocean in an outwardly extending eddy shape, indicating the influence of turbulence mixing and the transmission of ocean eddy energy (Wyrtki et al., 1976). Mesoscale eddies are widely present in the global ocean and dominate the ocean's kinetic energy. They are also involved in energy cascade at different scales (Shang et al., 2013). Clayton et al. (2013) proposed that increasing the resolution of physical models can enhance dispersal rates by narrowing and accelerating boundary currents, resolving swift transports associated with eddy stirring. To better illustrate the dynamic process of the transport and mixing of HgPR, we create global and regional videos using data from the entire simulation period (Fig. S6 and Fig. S7). The results show that HgPR spreads outward in an eddy shape, driven by HgPR concentrations and influenced by the kinetic energy transmission

by ocean eddies and the mixing of turbulence. This further emphasizes the important role of eddy-driven processes and turbulence mixing, in the transport and distribution of riverine Hg in coastal and shelf regions.

3.3 Impact of Biological Pump

The spatial distribution of modeled Hg_{aq}^{P} sinking flux (Figure 6c) follows the distribution of POC out of the euphotic zone

265   (Fig. S3). Globally, the Hg_{aq}^{P} sinking flux from the surface (0-10m) is 1.12 mol a^{-1}. The POC pool encompasses both detritus and living phytoplankton in aquatic food webs. Phytoplankton is known to accumulate Hg from their surrounding aqueous environment and is considered to be the primary entry point for Hg into marine food chains (Pickhardt and Fisher, 2007). The modeled distributions of all phytoplankton and zooplankton biomass in the euphotic zone are shown in Figures 6a and 6d, respectively. And the modeled distributions of phytoplankton and zooplankton are consistent with previous model results and

270   observations (Kuhn et al., 2019; Wu et al., 2020). The distribution of surface chlorophyll concentrations (Figure 6b) also aligns well with the phytoplankton distribution. The model simulates elevated sinking flux of HgP in high-latitude oceans of the northern hemisphere due to enhanced nutrient input from terrestrial erosion, in the equatorial region of the Southern Ocean, and along the west coasts of continents with strong upwelling.
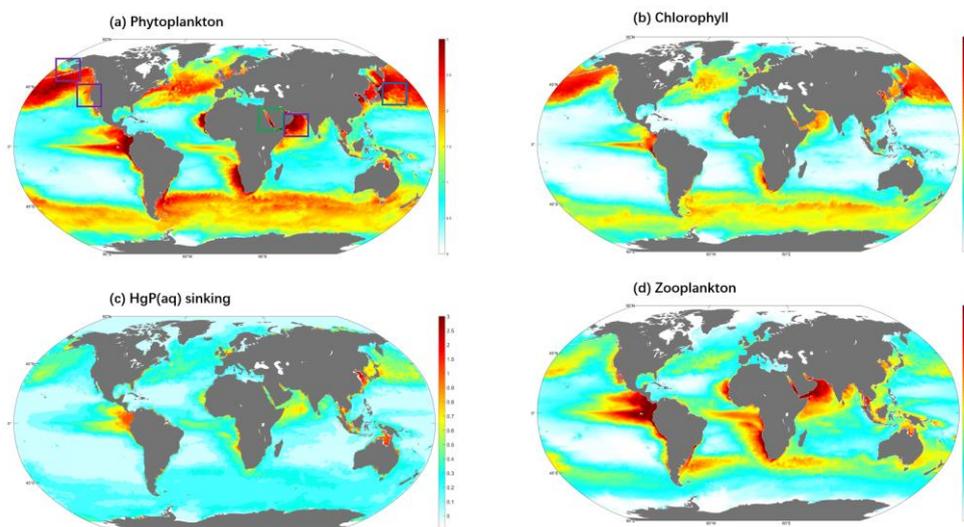
275   **Figure 6. Global distribution of the daily mean ecological variables (0-10m). (a) the sum of 35 kinds of biomass (in carbon content) concentration of phytoplankton, $mmol\ C\ m^{-3}$), the areas highlighted by boxes are possible algal regions, and the green box area is the final selected algal region; (b) the sum of 35 kinds of surface chlorophyll concentrations (color, unit $mg\ chl\ a\ m^{-3}$); (c) HgP(aq) sinking flux (color, unit $fM\ m^{-2}\ s^{-1}$); (d) the sum of 16 kinds of biomass (in carbon content) concentration of zooplankton, unit $mmol\ C\ m^{-3}$).**

280   Online biogeochemistry makes Hg more sensitive to environmental changes at shorter time scales. In our study, we try to establish a correlation between plankton and the sinking of particle-bound Hg. To achieve this, we need to observe and compare the changes in the HgP sinking flux during periods when plankton undergo significant fluctuations. One such process is algal bloom caused by eutrophication. Eutrophication is the process by which the primary production in a water body increases, in severe cases can lead to large blooms of algal. Algal bloom mostly occurs in coastal areas, Dai et al. (2023) found that algal

285   blooms occurred in 126 out of the 153 coastal countries examined. These blooms can significantly affect the biogeochemistry in the water column, including the distribution and cycling of nutrients, organic matter, and other elements, including Hg. The decomposition of algal debris can increase the flux of particulate organic matter (Macalady et al., 2000) and associated Hg to the sediments. Furthermore, the uptake of Hg by phytoplankton can also increase during algal blooms, which can lead to higher Hg concentrations in the sinking organic matter. Investigating the changes in the HgP sinking flux during algal blooms can

290   provide valuable insights into the biogeochemical processes controlling the fate and transport of Hg in aquatic systems.

We identify algal bloom events on a global scale for the simulated period. The ICES meeting (1984) concluded that a bloom is a deviation from the normal phytoplankton mass. Therefore, we can design such an algorithm to detect algal bloom events: during the simulated period, an algal bloom event is if it has the largest deviation from the average in a certain range of time. In this way, we capture 5 possible bloom regions, located in the Red Sea (detected region's center position:34.4°E, 26.2°N),

295   the Northwest Pacific (155.5°E, 33.4°N), the Bering Strait (171.2°W, 67.5°N), the west coast of the United States (124.5°W, 42.2°N), and the southern coast of the Arabian Peninsula (52.2°W, 15.4°N), respectively (Figure 6a). Upon analyzing the time series data, we observe significant fluctuations and peaks in the phytoplankton biomass at two regions, Point A in the northwestern Red Sea and Point B in the northwest Pacific Ocean (Figure 7). To further confirm that these fluctuations are indeed bloom events, we examine the nutrient levels of nitrogen and phosphorus in the water at the two regions (Fig. S4). As

300   elevated nitrogen and phosphorus elements are known to be associated with eutrophication and algal blooms, we find that the nutrient levels at Point A are above the average during the peak days, suggesting that the occurrence of algal blooms here. It is possibly attributed to higher sea surface temperature or increased use of nitrogen fertilizers in neighboring countries such as Egypt, and Saudi Arabia (Ritchie et al., 2022), both of which can contribute to the blooms (Dai et al., 2023). Previous research has also reported algal bloom events in the Red Sea (Mohamed, 2018). The intense fluctuations in phytoplankton biomass at

305   Point A during the bloom period (possibly between mid-March and early May) are indicative of a bloom event, as shown by the abrupt peaks in plankton biomass, chlorophyll concentration, and Hg_{aq}^P sinking flux, all of which are significantly higher than the average (Figure 7).
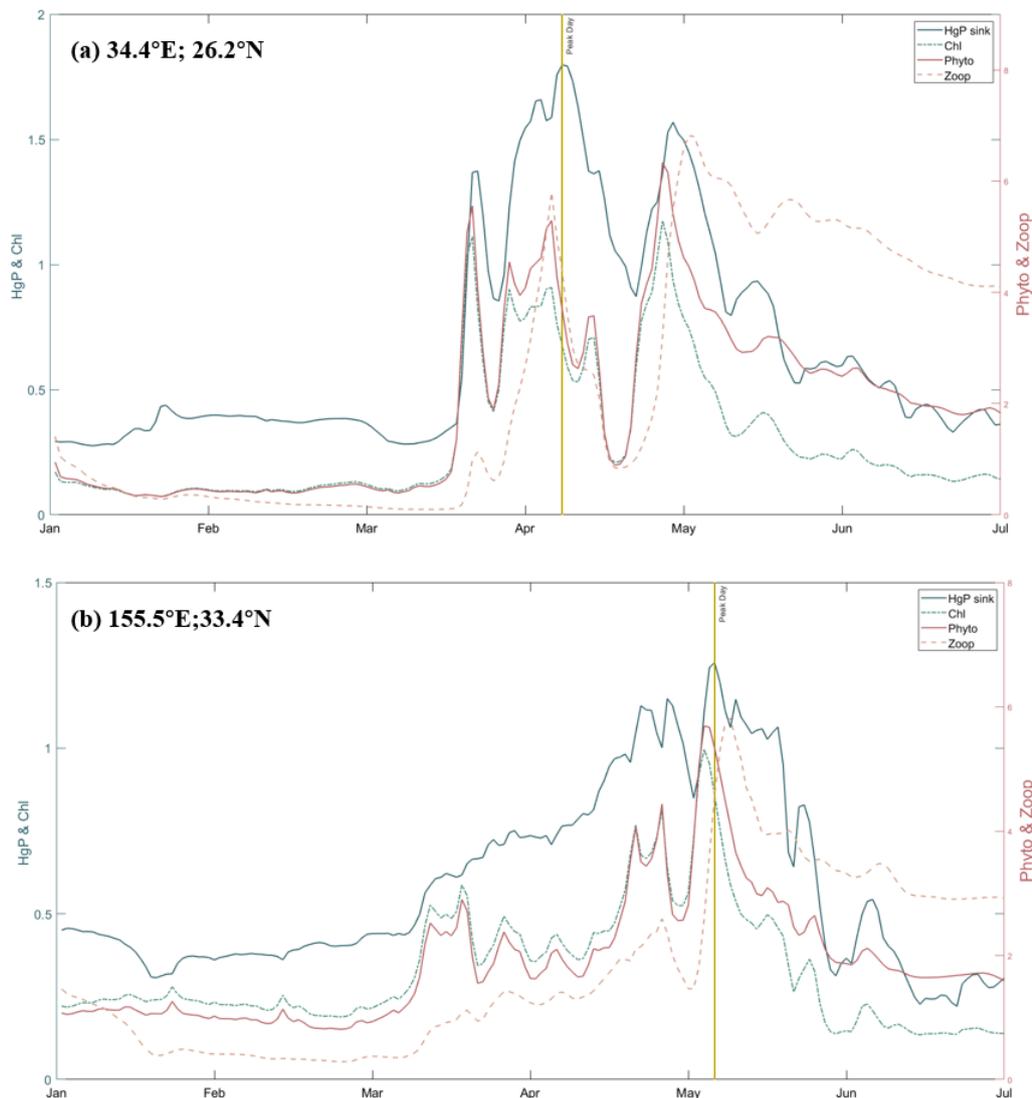
Figure 7. Time-series of HgP(aq) sinking flux ($fM\ m^{-2}\ s^{-1}$), the sum of 35 kinds of surface chlorophyll concentrations
(mg chl a m^{-3}), the sum of 35 kinds of biomass concentration of phytoplankton and zooplankton ($mmol\ C\ m^{-3}$).

We determine the approximate extent of blooms by generating a global distribution of plankton, chlorophyll, and Hg^P_{aq} sinking flux on the peak day (Fig. S5). Our results indicate that the Point A bloom spanned two latitudes and two longitudes, possibly influenced by coastal topography. On the peak day of Point A bloom, the Hg^P_{aq} sinking flux is 2.7 times greater than the overall average and 5.2 times greater than the non-blooming mean. This suggests that the sinking of particle-bound Hg is influenced by ecological changes in seawater. During algal blooms, the increased phytoplankton biomass creates more particulate matter

to bind with Hg, leading to accelerated organic particle scavenging and remineralization in the water column. Thus, in this way, increase the sinking flux of particle-bound Hg after a short time. Our discovery was facilitated by integrating our model with online biogeochemistry, which promptly reflected the abrupt fluctuations in phytoplankton and enabled us to quickly observe changes in the sinking of Hg particles.

320 **4 Conclusions**

In this study, we estimate the global biogeochemical cycling of Hg in a state-of-the-art physical-ecosystem ocean model (High-resolution-MITgcm/Hg), realizing Hg transport in eddy-scale. One of the biggest advantages of our model is the promoted resolution so that the small-scale changes of marine Hg can be captured. We use the online biogeochemistry fields to participate in the ocean transformation and reaction processes of Hg. Online biogeochemistry is involved in the reaction between
325 elemental Hg and divalent, and the process of particle-Hg forming as well as the remineralization processes. The coupling with the Darwin project further enhances the specificity of the Hg biogeochemistry in the MITgcm model. Overall, this approach provides a comprehensive understanding of the global biogeochemical cycling of Hg and its interactions with the marine ecosystem.

The horizontal resolution of 18km allows our model to simulate the turbulence, which is omitted in previous global models.
330 Turbulent mixing and shear effects affect the transport of materials (including Hg) in the ocean, so only a high enough resolution can refine this physical process. With this advanced physical configuration, we introduce the latest river discharge inventory from Liu et al. (2021) and 12 nutrients exported by river from WaterSheds 2 (Mayorga et al., 2010). Our high-resolution model provides a more detailed depiction of the fate of riverine Hg discharged to the global oceans.

The ocean plays a critical role in the global Hg cycle, and the large size of the ocean is a major site for atmospheric mercury
335 transport, transformation, and deposition. Global ocean models of Hg require a better understanding of biogeochemical controls on Hg speciation. We qualitatively analyzed the biogeochemistry effect on the particle scavenging process of inorganic Hg. The high-resolution MITgcm can help us better predict the transport and fate of Hg in the ocean and its impact on the global Hg cycle. This provides us with more advanced tools and methods to address natural and human-disturbing global Hg e Data availability. The data supporting the findings of this study are available within the article and its Supplement.
340

Code availability. The MITgcm model code is available at https://github.com/MITgcm/MITgcm.git. The code of MITgcm-ECCO2-Hg in this paper is permanently archived on Zenodo at https://doi.org/10.5281/zenodo.7932859 (Zhu and Zhang, 2023).

345 Data availability. The data supporting the findings of this study are available within the article and its Supplement.

Author contribution. Zhang Y and Zhu S conceived the idea and designed the model experiments. Zhang Y and Jahn O developed high-resolution MITgcm model. Zhu S and Zhang Y modified the code of the MITgcm-ECCO2-Hg model. Wu P and Zhang S improved part of the code. Zhu S performed the simulations, conducted the analysis, and wrote the paper. Zhang Y and Zhu S edited the paper.

Competing interests. The contact author has declared that neither they nor their co-author has any competing interests.

Acknowledgment. We thank the financial support from the National Natural Science Foundation of China (NNSFC) 42177349, the Fundamental Research Funds for the Central Universities (grant no. 0207-14380188, 0207-14380168), Frontiers Science Center for Critical Earth Material Cycling, and the Collaborative Innovation Center of Climate Change, Jiangsu Province.

References

Adcroft, A., Campin, J. M., Hill, C., and Marshall, J.: Implementation of an atmosphere-ocean general circulation model on the expanded spherical cube, Monthly Weather Review, 132, 2845-2863, 10.1175/mwr2823.1, 2004.

Amorim, C. A. and Moura, A. D.: Ecological impacts of freshwater algal blooms on water quality, plankton biodiversity, structure, and ecosystem functioning, Science of the Total Environment, 758, 10.1016/j.scitotenv.2020.143605, 2021.

Amos, H. M., Jacob, D. J., Kocman, D., Horowitz, H. M., Zhang, Y., Dutkiewicz, S., Horvat, M., Corbitt, E. S., Krabbenhoft, D. P., and Sunderland, E. M.: Global biogeochemical implications of mercury discharges from rivers and sediment burial, Environ Sci Technol, 48, 9514-9522, 10.1021/es502134t, 2014.

Amos, H. M., Jacob, D. J., Holmes, C. D., Fisher, J. A., Wang, Q., Yantosca, R. M., Corbitt, E. S., Galarneau, E., Rutter, A. P., Gustin, M. S., Steffen, A., Schauer, J. J., Graydon, J. A., St Louis, V. L., Talbot, R. W., Edgerton, E. S., Zhang, Y., and Sunderland, E. M.: Gas-particle partitioning of atmospheric Hg(II) and its effect on global mercury deposition, Atmospheric Chemistry and Physics, 12, 591-603, 10.5194/acp-12-591-2012, 2012.

Amyot, M., Gill, G. A., and Morel, F. M. M.: Production and loss of dissolved gaseous mercury in coastal seawater, Environmental Science & Technology, 31, 3606-3611, 10.1021/es9703685, 1997.

Andersson, M. E., Sommar, J., Gardfeldt, K., and Jutterstrom, S.: Air-sea exchange of volatile mercury in the North Atlantic Ocean, Marine Chemistry, 125, 1-7, 10.1016/j.marchem.2011.01.005, 2011.

Bieser, J. and Schrum, C.: Impact of marine mercury cycling on coastal atmospheric mercury concentrations in the North- and Baltic Sea region, Elementa-Science of the Anthropocene, 4, 10.12952/journal.elementa.000111, 2016.

Bieser, J., Amptmeijer, D., Daewel, U., Kuss, J., Soerensen, A. L., and Schrum, C.: The 3D biogeochemical marine mercury cycling model MERCY v2. 0–linking atmospheric Hg to methyl mercury in fish, Geoscientific Model Development Discussions, 1-59, 2022.

380   Bowman, K. L., Hammerschmidt, C. R., Lamborg, C. H., and Swarr, G.: Mercury in the North Atlantic Ocean: The US GEOTRACES zonal and meridional sections, Deep-Sea Research Part Ii-Topical Studies in Oceanography, 116, 251-261, 10.1016/j.dsr2.2014.07.004, 2015.

Chaulk, A., Stern, G. A., Armstrong, D., Barber, D. G., and Wang, F.: Mercury Distribution and Transport Across the Ocean-Sea-Ice-Atmosphere Interface in the Arctic Ocean, Environmental Science & Technology, 45, 1866-1872, 10.1021/es103434c,

385   2011.

Ci, Z., Zhang, X., Yin, Y., Chen, J., and Wang, S.: Mercury Redox Chemistry in Waters of the Eastern Asian Seas: From Polluted Coast to Clean Open Ocean, Environmental Science & Technology, 50, 2371-2380, 10.1021/acs.est.5b05372, 2016.

Clayton, S., Dutkiewicz, S., Jahn, O., and Follows, M. J.: Dispersal, eddies, and the diversity of marine phytoplankton, Limnology and Oceanography: Fluids and Environments, 3, 182-197, 2013.

390   Cossa, D., Heimbuerger, L.-E., Lannuzel, D., Rintoul, S. R., Butler, E. C. V., Bowie, A. R., Averty, B., Watson, R. J., and Remenyi, T.: Mercury in the Southern Ocean, Geochimica Et Cosmochimica Acta, 75, 4037-4052, 10.1016/j.gca.2011.05.001, 2011.

Costa, M. and Liss, P. S.: Photoreduction of mercury in sea water and its possible implications for Hg-0 air-sea fluxes, Marine Chemistry, 68, 87-95, 10.1016/s0304-4203(99)00067-5, 1999.

395   Dai, Y., Yang, S., Zhao, D., Hu, C., Xu, W., Anderson, D. M., Li, Y., Song, X. P., Boyce, D. G., Gibson, L., Zheng, C., and Feng, L.: Coastal phytoplankton blooms expand and intensify in the 21st century, Nature, 10.1038/s41586-023-05760-y, 2023.

Dutkiewicz, S., Follows, M. J., and Bragg, J. G.: Modeling the coupling of ocean ecology and biogeochemistry, Global Biogeochemical Cycles, 23, 10.1029/2008gb003405, 2009.

Fitzgerald, W. F., Lamborg, C. H., and Hammerschmidt, C. R.: Marine biogeochemical cycling of mercury, Chemical Reviews,

400   107, 641-662, 10.1021/cr050353m, 2007.

Gardfeldt, K., Sommar, J., Stromberg, D., and Feng, X. B.: Oxidation of atomic mercury by hydroxyl radicals and photoinduced decomposition of methylmercury in the aqueous phase, Atmospheric Environment, 35, 3039-3047, 10.1016/s1352-2310(01)00107-8, 2001.

Heimbuerger, L.-E., Sonke, J. E., Cossa, D., Point, D., Lagane, C., Laffont, L., Galfond, B. T., Nicolaus, M., Rabe, B., and

405   van der Loeff, M. R.: Shallow methylmercury production in the marginal sea ice zone of the central Arctic Ocean, Scientific Reports, 5, 10.1038/srep10318, 2015.

Horowitz, H. M., Jacob, D. J., Zhang, Y., Dibble, T. S., Slemr, F., Amos, H. M., Schmidt, J. A., Corbitt, E. S., Marais, E. A., and Sunderland, E. M.: A new mechanism for atmospheric mercury redox chemistry: implications for the global mercury budget, Atmospheric Chemistry and Physics, 17, 6353-6371, 10.5194/acp-17-6353-2017, 2017.

410   Huang, S. and Zhang, Y.: Interannual Variability of Air-Sea Exchange of Mercury in the Global Ocean: The "Seesaw Effect" in the Equatorial Pacific and Contributions to the Atmosphere, Environ Sci Technol, 55, 7145-7156, 10.1021/acs.est.1c00691, 2021.

Jonsson, S., Andersson, A., Nilsson, M. B., Skyllberg, U., Lundberg, E., Schaefer, J. K., Akerblom, S., and Bjorn, E.: Terrestrial discharges mediate trophic shifts and enhance methylmercury accumulation in estuarine biota, Science Advances,
415   3, 10.1126/sciadv.1601239, 2017.

Kirk, J. L., Louis, V. L. S., Hintelmann, H., Lehnherr, I., Else, B., and Poissant, L.: Methylated Mercury Species in Marine Waters of the Canadian High and Sub Arctic, Environmental Science & Technology, 42, 8367-8373, 10.1021/es801635m, 2008.

Kuhn, A. M., Dutkiewicz, S., Jahn, O., Clayton, S., Rynearson, T. A., Mazloff, M. R., and Barton, A. D.: Temporal and Spatial
420   Scales of Correlation in Marine Phytoplankton Communities, Journal of Geophysical Research: Oceans, 124, 9417-9438, 10.1029/2019jc015331, 2019.

Kuss, J., Zulicke, C., Pohl, C., and Schneider, B.: Atlantic mercury emission determined from continuous analysis of the elemental mercury sea-air concentration difference within transects between 50 degrees N and 50 degrees S, Global Biogeochemical Cycles, 25, 10.1029/2010gb003998, 2011.

425   Lacerda, L. D.: Global mercury emissions from gold and silver mining, Water Air and Soil Pollution, 97, 209-221, 1997.

Laurier, F. J. G., Mason, R. P., Gill, G. A., and Whalin, L.: Mercury distributions in the North Pacific Ocean - 20 years of observations, Marine Chemistry, 90, 3-19, 10.1016/j.marchem.2004.02.025, 2004.

Lehnherr, I., St Louis, V. L., Hintelmann, H., and Kirk, J. L.: Methylation of inorganic mercury in polar marine waters, Nature Geoscience, 4, 298-302, 10.1038/ngeo1134, 2011.

430   Liu, M., Zhang, Q., Maavara, T., Liu, S., Wang, X., and Raymond, P. A.: Rivers as the largest source of mercury to coastal oceans worldwide, Nature Geoscience, 14, 672-677, 10.1038/s41561-021-00793-2, 2021.

Luengen, A. C. and Russell Flegal, A.: Role of phytoplankton in mercury cycling in the San Francisco Bay estuary, Limnology and Oceanography, 54, 23-40, 10.4319/lo.2009.54.1.0023, 2009.

Macalady, J. L., Mack, E. E., Nelson, D. C., and Scow, K. M.: Sediment microbial community structure and mercury
435   methylation in mercury-polluted Clear Lake, California, Applied and Environmental Microbiology, 66, 1479-1488, 10.1128/aem.66.4.1479-1488.2000, 2000.

Mason, R. P. and Sullivan, K. A.: The distribution and speciation of mercury in the South and equatorial Atlantic, Deep-Sea Research Part Ii-Topical Studies in Oceanography, 46, 937-956, 10.1016/s0967-0645(99)00010-7, 1999.

Mason, R. P., Lawson, N. M., and Sheu, G. R.: Mercury in the Atlantic Ocean: factors controlling air-sea exchange of mercury
440   and its distribution in the upper waters, Deep-Sea Research Part Ii-Topical Studies in Oceanography, 48, 2829-2853, 10.1016/s0967-0645(01)00020-0, 2001.

Mason, R. P., Reinfelder, J. R., and Morel, F. M. M.: BIOACCUMULATION OF MERCURY AND METHYLMERCURY, Water Air and Soil Pollution, 80, 915-921, 10.1007/bf01189744, 1995.

Mason, R. P., Rolfhus, K. R., and Fitzgerald, W. F.: Mercury in the North Atlantic, Marine Chemistry, 61, 37-53,
445   10.1016/s0304-4203(98)00006-1, 1998.

Mason, R. P., Hammerschmidt, C. R., Lamborg, C. H., Bowman, K. L., Swarr, G. J., and Shelley, R. U.: The air-sea exchange
of mercury in the low latitude Pacific and Atlantic Oceans, Deep-Sea Research Part I-Oceanographic Research Papers, 122,
17-28, 10.1016/j.dsr.2017.01.015, 2017.

Mason, R. P., Choi, A. L., Fitzgerald, W. F., Hammerschmidt, C. R., Lamborg, C. H., Soerensen, A. L., and Sunderland, E.
450   M.: Mercury biogeochemical cycling in the ocean and policy implications, Environmental Research, 119, 101-117,
10.1016/j.envres.2012.03.013, 2012.

Mayorga, E., Seitzinger, S. P., Harrison, J. A., Dumont, E., Beusen, A. H. W., Bouwman, A. F., Fekete, B. M., Kroeze, C.,
and Van Drecht, G.: Global Nutrient Export from WaterSheds 2 (NEWS 2): Model development and implementation,
Environmental Modelling & Software, 25, 837-853, 10.1016/j.envsoft.2010.01.007, 2010.

455   Menemenlis, D., Campin, J. M., Heimbach, P., Hill, C. N., Lee, T. S., Nguyen, A. T., Schodlok, M. P., and Zhang, H.: ECCO2:
High Resolution Global Ocean and Sea Ice Data Synthesis, 2008.

Mohamed, Z. A.: Potentially harmful microalgae and algal blooms in the Red Sea: Current knowledge and research needs,
Marine Environmental Research, 140, 234-242, 10.1016/j.marenvres.2018.06.019, 2018.

Monperrus, M., Tessier, E., Amouroux, D., Leynaert, A., Huonnic, P., and Donard, O. F. X.: Mercury methylation,
460   demethylation and reduction rates in coastal and marine surface waters of the Mediterranean Sea, Marine Chemistry, 107, 49-
63, 10.1016/j.marchem.2007.01.018, 2007.

Moura, R. L., Amado, G. M., Moraes, F. C., Brasileiro, P. S., Salomon, P. S., Mahiques, M. M., Bastos, A. C., Almeida, M.
G., Silva, J. M., Araujo, B. F., Brito, F. P., Rangel, T. P., Oliveira, B. C. V., Bahia, R. G., Paranhos, R. P., Dias, R. J. S., Siegle,
E., Figueiredo, A. G., Pereira, R. C., Leal, C. V., Hajdu, E., Asp, N. E., Gregoracci, G. B., Neumann-Leitao, S., Yager, P. L.,
465   Francini, R. B., Froes, A., Campeao, M., Silva, B. S., Moreira, A. P. B., Oliveira, L., Soares, A. C., Araujo, L., Oliveira, N. L.,
Teixeira, J. B., Valle, R. A. B., Thompson, C. C., Rezende, C. E., and Thompson, F. L.: An extensive reef system at the
Amazon River mouth, Science Advances, 2, 10.1126/sciadv.1501252, 2016.

Moye, H. A., Miles, C. J., Phlips, E. J., Sargent, B., and Merritt, K. K.: Kinetics and untake mechanisms for
monomethylmercury between freshwater algae and water, Environmental Science & Technology, 36, 3550-3555,
470   10.1021/es011421z, 2002.

Nightingale, P. D., Malin, G., Law, C. S., Watson, A. J., Liss, P. S., Liddicoat, M. I., Boutin, J., and Upstill-Goddard, R. C.:
In situ evaluation of air-sea gas exchange parameterizations using novel conservative and volatile tracers, Global
Biogeochemical Cycles, 14, 373-387, 10.1029/1999gb900091, 2000.

Nriagu, J. O.: LEGACY OF MERCURY POLLUTION, Nature, 363, 589-589, 10.1038/363589a0, 1993.

475   Obrist, D., Kirk, J. L., Zhang, L., Sunderland, E. M., Jiskra, M., and Selin, N. E.: A review of global environmental mercury
processes in response to human and natural perturbations: Changes of emissions, climate, and land use, Ambio, 47, 116-140,
10.1007/s13280-017-1004-9, 2018.

Outridge, P. M., Mason, R. P., Wang, F., Guerrero, S., and Heimburger-Boavida, L. E.: Updated Global and Oceanic Mercury Budgets for the United Nations Global Mercury Assessment 2018, Environmental Science & Technology, 52, 11466-11477, 480   10.1021/acs.est.8b01246, 2018.

Pacyna, E. G., Pacyna, J. M., Sundseth, K., Munthe, J., Kindbom, K., Wilson, S., Steenhuisen, F., and Maxson, P.: Global emission of mercury to the atmosphere from anthropogenic sources in 2005 and projections to 2020, Atmospheric Environment, 44, 2487-2499, 10.1016/j.atmosenv.2009.06.009, 2010.

Pickhardt, P. C. and Fisher, N. S.: Accumulation of inorganic and methylmercury by freshwater phytoplankton in two 485   contrasting water bodies, Environmental Science & Technology, 41, 125-131, 10.1021/es060966w, 2007.

Ritchie, H., Roser, M., and Rosado, P.: Fertilizers, Our World in Data, https://ourworldindata.org/fertilizers, 2022.

Rolfhus, K. R. and Fitzgerald, W. F.: The evasion and spatial/temporal distribution of mercury species in Long Island Sound, CT-NY, Geochimica Et Cosmochimica Acta, 65, 407-418, 10.1016/s0016-7037(00)00519-6, 2001.

Rosati, G., Canu, D., Lazzari, P., and Solidoro, C.: Assessing the spatial and temporal variability of methylmercury 490   biogeochemistry and bioaccumulation in the Mediterranean Sea with a coupled 3D model, Biogeosciences, 19, 3663-3682, 10.5194/bg-19-3663-2022, 2022.

Sarmiento, J. L., Gruber, N., Brzezinski, M. A., and Dunne, J. P.: High-latitude controls of thermocline nutrients and low latitude biological productivity, Nature, 427, 56-60, 10.1038/nature02127, 2004.

Selin, N. E., Jacob, D. J., Yantosca, R. M., Strode, S., Jaegle, L., and Sunderland, E. M.: Global 3-D land-ocean-atmosphere 495   model for mercury: Present-day versus preindustrial cycles and anthropogenic enrichment factors for deposition (vol 22, artn no GB3099, 2008), Global Biogeochemical Cycles, 22, 10.1029/2008gb003282, 2008.

Semeniuk, K. and Dastoor, A.: Development of a global ocean mercury model with a methylation cycle: Outstanding issues, Global Biogeochemical Cycles, 31, 400-433, 10.1002/2016gb005452, 2017.

Shang, X.-d., Xu, C., Chen, G.-y., and Lian, S.-m.: Review on mechanical energy of ocean mesoscale eddies and associated 500   energy sources and sinks, Journal of Tropical Oceanography, 32, 24-36, 10.3969/j.issn.1009-5470.2013.02.003, 2013.

Soerensen, A. L., Mason, R. P., Balcom, P. H., and Sunderland, E. M.: Drivers of Surface Ocean Mercury Concentrations and Air-Sea Exchange in the West Atlantic Ocean, Environmental Science & Technology, 47, 7757-7765, 10.1021/es401354q, 2013.

Soerensen, A. L., Sunderland, E. M., Holmes, C. D., Jacob, D. J., Yantosca, R. M., Skov, H., Christensen, J. H., Strode, S. A., 505   and Mason, R. P.: An Improved Global Model for Air-Sea Exchange of Mercury: High Concentrations over the North Atlantic, Environmental Science & Technology, 44, 8574-8580, 10.1021/es102032g, 2010.

Sonke, J. E., Teisserenc, R., Heimburger-Boavida, L.-E., Petrova, M. V., Maruszak, N., Le Dantec, T., Chupakov, A. V., Li, C., Thackray, C. P., Sunderland, E. M., Tananaev, N., and Pokrovsky, O. S.: Eurasian river spring flood observations support net Arctic Ocean mercury export to the atmosphere and Atlantic Ocean, Proceedings of the National Academy of Sciences of 510   the United States of America, 115, E11586-E11594, 10.1073/pnas.1811957115, 2018.

Streets, D. G., Devane, M. K., Lu, Z., Bond, T. C., Sunderland, E. M., and Jacob, D. J.: All-Time Releases of Mercury to the Atmosphere from Human Activities, Environmental Science & Technology, 45, 10485-10491, 10.1021/es202765m, 2011.

Strode, S., Jaegle, L., and Emerson, S.: Vertical transport of anthropogenic mercury in the ocean, Global Biogeochemical Cycles, 24, 10.1029/2009gb003728, 2010.

515 Strode, S. A., Jaegle, L., Selin, N. E., Jacob, D. J., Park, R. J., Yantosca, R. M., Mason, R. P., and Slemr, F.: Air-sea exchange in the global mercury cycle, Global Biogeochemical Cycles, 21, 10.1029/2006gb002766, 2007.

Ward, B. A., Dutkiewicz, S., and Follows, M. J.: Modelling spatial and temporal patterns in size-structured marine plankton communities: top-down and bottom-up controls, Journal of Plankton Research, 36, 31-47, 10.1093/plankt/fbt097, 2014.

Watras, C. J., Back, R. C., Halvorsen, S., Hudson, R. J. M., Morrison, K. A., and Wente, S. P.: Bioaccumulation of mercury 520 in pelagic freshwater food webs, Science of the Total Environment, 219, 183-208, 10.1016/s0048-9697(98)00228-9, 1998.

Wu, P., Zakem, E. J., Dutkiewicz, S., and Zhang, Y.: Biomagnification of Methylmercury in a Marine Plankton Ecosystem, Environ Sci Technol, 54, 5446-5455, 10.1021/acs.est.9b06075, 2020.

Wunsch, C. and Ferrari, R.: Vertical mixing, energy and thegeneral circulation of the oceans, Annual Review of Fluid Mechanics, 36, 281-314, 10.1146/annurev.fluid.36.050802.122121, 2004.

525 Wyrtki, K., Magaard, L., and Hager, J.: Eddy energy in the oceans, Journal of Geophysical Research, 81, 2641-2646, 10.1029/JC081i015p02641, 1976.

Zhang, P. and Zhang, Y.: Earth system modeling of mercury using CESM2 – Part 1: Atmospheric model CAM6-Chem/Hg v1.0, Geoscientific Model Development, 15, 3587-3601, 10.5194/gmd-15-3587-2022, 2022.

Zhang, Y., Jaegle, L., and Thompson, L.: Natural biogeochemical cycle of mercury in a global three-dimensional ocean tracer 530 model, Global Biogeochemical Cycles, 28, 553-570, 10.1002/2014gb004814, 2014a.

Zhang, Y., Jaegle, L., Thompson, L., and Streets, D. G.: Six centuries of changing oceanic mercury, Global Biogeochemical Cycles, 28, 1251-1261, 10.1002/2014gb004939, 2014b.

Zhang, Y., Soerensen, A. L., Schartup, A. T., and Sunderland, E. M.: A Global Model for Methylmercury Formation and Uptake at the Base of Marine Food Webs, Global Biogeochemical Cycles, 34, 10.1029/2019gb006348, 2020.

535 Zhang, Y., Song, Z., Huang, S., Zhang, P., Peng, Y., Wu, P., Gu, J., Dutkiewicz, S., Zhang, H., Wu, S., Wang, F., Chen, L., Wang, S., and Li, P.: Global health effects of future atmospheric mercury emissions, Nat Commun, 12, 3035, 10.1038/s41467-021-23391-7, 2021.

Zhang, Y. X., Jacob, D. J., Dutkiewicz, S., Amos, H. M., Long, M. S., and Sunderland, E. M.: Biogeochemical drivers of the fate of riverine mercury discharged to the global and Arctic oceans, Global Biogeochemical Cycles, 29, 854-864, 540 10.1002/2015gb005124, 2015.